# Cross-kingdom regulation of tRNAs/tRFs derived from Chinese yew

Kai-Yue Cao[1,2†], Tong-Meng Yan[1,2†], Ji-Zhou Zhang[3], Ting-Fung Chan[3], Jie Li[4], Chong Li[4], Elaine Lai-Han Leung[1,2], Zhi-Hong Jiang[1,2]*

[1]State Key Laboratory of Quality Research in Chinese Medicine, Macau University of Science and Technology, Macau SAR, China.

[2]Macau Institute for Applied Research in Medicine and Health, Macau University of Science and Technology, Macau SAR, China.

[3]School of Life Sciences, and State Key Laboratory of Agrobiotechnology, The Chinese University of Hong Kong, Shatin, Hong Kong SAR, China.

[4]College of Pharmaceutical Sciences, Southwest University, Chongqing 400715, P. R. China.

***Corresponding author**: Dr. Zhi-Hong Jiang, State Key Laboratory of Quality Research in Chinese Medicine, Macau University of Science and Technology, Avenida Wai Long, Taipa, Macau SAR, China.

**E-mail**: zhjiang@must.edu.mo (Zhi-Hong Jiang)

[†]These authors contributed equally to this work.

**Plants containing countless chemical constituent have benefited mankind since the origin of life. Although secondary metabolites in plants, such as morphine, artemisinin and taxol, have been developed as therapeutic drugs for clinical therapy, few study focuses on the pharmacological activities of plant small RNAs with function of cross-kingdom regulations. Yew is widely considered as a "superstar" plant due to the discovery of paclitaxel, or taxol, which is a well-known natural drug for the treatment of multiple types of cancer[1]. Here we show the surprising finding that an RNA fragment, named tRF-T11, derived from $tRNA^{His(GUG)}$ of Chinese yew strongly suppressed human ovarian cancer progression. In A2780 cells, tRF-T11 mimic (a double-stranded RNA with tRF-T11 as antisense chain) exhibited potent cytotoxicity comparable to that of taxol, but no significant cytotoxicity to normal ovarian surface epithelial cells. Moreover, the cytotoxicity of tRF-T11 mimic is 80-fold stronger than that of taxol in taxol-resistant A2780 cells. Bioinformatic and molecular biological studies revealed that tRF-T11 targets transient receptor potential cation channel subfamily A member 1 (*TRPA1*) to inhibit its expression levels. In a further *in***

***vivo* investigation, the growth rate of ovarian tumor xenografts in nude mice was significantly reduced by treatment with tRF-T11 mimic, and the *TRPA1* protein expression in tumors treated with tRF-T11 mimic was also down-regulated. Our findings are the first to provide evidence that plant-derived tRFs can regulate the expression of target genes *in vitro* and *in vivo*, indicating that they may become as a new source of druggable siRNA. Moreover, this discovery demonstrated a pilot example of an innovative approach for not only identifying pharmacologically-active tRFs from plants, but also for improving the efficiency and possibilities of discovering new drug target.**

Plants have provided mankind with an important source of medicinal products for millennia. Throughout ancient history, humans learned to harness herbal decoctions for disease prevention and treatment. Today, thousands of secondary metabolites, such as flavonoids, terpenes and alkaloids, from this chemical treasure have been identified as active compounds. Intriguingly, crude plant extracts were more effective than the synthetic versions of phytochemicals, implying that whole plant extracts contain a cocktail of products in which substances like macromolecules

other than small molecules may contribute to the overall pharmacological effects[2]. However, few study has been performed on the pharmacological activity of plant macromolecules excluding polysaccharides because they are considered inactive, nonabsorbable and unstable in human body, such as RNA, DNA and proteins. Small RNAs (<200 nt) were found to play critical roles in a wide range of biological processes in microorganisms, plants, animals and human, and to participate in a variety of human diseases by regulating protein-coding genes[3,4]. Since the first evidence that plant-derived miRNAs can regulate gene expression in mammalian systems was provided by Zhang *et al*[5] in 2012, many other miRNAs from small RNAs in plants have been extensively studied for their cross-kingdom regulatories[6-9]. These findings suggested the promise of small RNAs from plants to be developed as therapeutic agents. A recent report by Shekhawat[10] showed that the small RNA of corn exhibited appreciable antiproliferative activity toward HeLa cells, implying the possibility that small RNA species with larger molecular weight than miRNA play regulatory roles. In fact, as the most abundant small RNA species expressed in all living organisms, transfer RNAs (tRNAs) play a well-defined role in protein

translation and perform diverse regulatory functions in some important biological processes, such as cell signaling, apoptosis modulation and stress response programs[11]. Recently, tRNA-derived fragments (tRFs) have also been recognized to play regulatory roles[12]. This class of small RNAs is non-randomly generated from tRNAs, and many are specifically and abundantly produced under particular conditions, such as cancer and viral infection[13,14]. Some studies have also revealed that the expression of several tRFs is positively correlated with cell proliferation in different cancer cell lines[15], suggesting that tRFs and their related signaling pathways could be novel targets for intervention in the treatment of cancers. These findings prompted us to consider the further possibility that in addition to well-established players such as miRNAs and small molecules in plants, tRNAs and their fragments, which account for overwhelming majority of small RNA species in plants, may hold great potential as biological regulators in mammals. Below, we describe the first study of the pharmacological activities of tRNAs and tRFs derived from Chinese yew (*Taxus chinensis*) and identification of their molecular target.

Total RNA with high integrity (RIN=7.7) and purity (A260/280=2.08, A260/230=2.00; Supplementary Fig 1a) was isolated from fresh branches of *T. chinensis* by using a well-developed CTAB method (Supplementary Fig 1b, c), in which small RNA was separated from large RNA with high purity (<200 nt, Supplementary Fig 2). The tRNAs were then gel fractionated and purified (Supplementary Fig 3a) to successfully delete 5S and 5.8S rRNA and other RNA species (Supplementary Fig 3b). Sequence information and the proportion of each type of RNA in this tRNA-enriched fraction (tEF) were determined by performing next-generation sequencing (NGS). As shown in Fig 1c and Supplementary Table 1, over 1.7 million clean reads distributed mainly from 60 to 80 mer were generated, and over 20 individual tRNA sequences were identified, which accounted for approximately 14% of the overall number of reads in the tEF library (Fig 1d). The cytotoxicity of the tEF was investigated using an MTT assay on the A2780 human ovarian cancer (OVCA) cell line. The $IC_{50}$ value for dose-dependent growth inhibition of A2780 cells *in vitro* was 128.8 nM when the tEF was well encapsulated and delivered via liposomes, while no significant cytotoxicity of the tEF was observed

without transfection (Fig 1a, b), implying that tRNAs or their fragments in the tEF might act as effectors. Furthermore, when rRNA degradation fragments (Fig 1e) were removed from the tEF samples via a Ribo-Zero rRNA removal kit (Illumina), the retained tRNA species induced the death of A2780 cells with increased efficiency (Fig 1f), indicating the major contribution of tRNA species to the overall cytotoxic effects of the tEF. Subsequently, the five most abundant (>500 reads per million) individual tRNAs were purified from small RNA of *T. chinensis* by using a magnetic solid-phase DNA probe method[16] and were identified by ultra-high performance liquid chromatography coupled with quadrupole time-of-flight mass spectrometry (Fig 1g-i). Cytotoxicity of purified tRNAs was then investigated on A2780 cells, HepG2 of liver cancer and MCF-7 of breast cancer cells. As a result, A2780 and HepG2 cells exhibited a proliferation reduction of over 75% when treated with individual tRNAs at 25 nM (Fig 1j, k), while MCF-7 cells were much less sensitive (reduction of less than 30%) to these tRNA molecules. This pattern corresponded to an approximate $IC_{50}$ value of 14.3 nM for the growth inhibition of A2780 cells caused by treatment with $tRNA^{Trp(CCA)}$ for 48 h, which is close to that of taxol (7.4 nM) used

as a positive control drug (Fig 1l). This provides the first evidence of pharmacological activities of plant-derived tRNAs, suggesting that they are a new class of therapeutic agents from medicinal plants.

Meanwhile, since the previous study has revealed that the tRFs could regulate endogenous gene in breast cancer cells[15], we hypothesized that tRF from the above cytotoxic tRNAs of Chinese yew may be pharmacologically-active. Indeed, tRFs from the 5' terminal and 3' ends (5'-tRF and 3'-tRF, respectively) are the most abundant tRFs associated with the AGO protein, which is a key component of the RNA interference pathway[17]. A similar report showed that a 5'-tRF of 19 nucleotides is the most abundant tRF in land plants[18]. Thus, 36 tRFs derived from the top 9 abundant tRNAs of Chinese yew, including 5'-tRF and 3'-tRF with lengths of 22 and 19 nt, respectively, were selected as antisense strands of tRF mimics in siRNA form (Fig 2a, Supplementary Table 2), and the antiproliferative activities of these tRF mimics against A2780 and its taxol-resistant strain (A2780T) cells were screened. The results showed that two of these 36 tRF mimics significantly inhibited the proliferation of the A2780 cells by over 50% at 50 nM (Fig 2b). Among these tRF

mimics, tRF-T11 mimic (a double strand RNA with a 22 nt 5'-tRF derived from $tRNA^{His(GUG)}$ as antisense RNA) showed the highest antiproliferative activity against both cell lines. As shown in Fig 2c, the $IC_{50}$ value of tRF-T11 mimic for inhibiting the growth of A2780 cells was 31 nM, which is comparable to that of taxol (10.2 nM). Surprisingly, high sensitivity to tRF-T11 mimic was also observed in A2780T cells, corresponding to an $IC_{50}$ value of 32 nM, which is 80-fold lower than that of taxol (2600 nM). In addition, no significant cytotoxicity of tRF-T11 mimic to IOSE80 normal ovarian surface epithelial cells was observed. Furthermore, the cytotoxicity of tRF-T11 mimic was confirmed by visualizing and tracking fluorescent dye (FAM)-labeled tRF-T11 mimic in A2780 cells. The images shown in Fig 2d indicated that tRF-T11 mimic was efficiently transfected into the cytoplasm of A2780 cells, where they exhibited functions involved in the biological processes, such as suppressing the expression of endogenous targets[19]. These results indicated that *Taxus*-derived tRFs are promising therapeutic agents for drug-resistant OVCA.

The divergent activity of tRF mimics derived from individual tRNAs observed in this study suggested that plant-derived tRFs can exhibit bioactivities in a

146 sequence-specific manner in mammalian cells. It has been reported that functionality
147 of exogenous tRFs possibly overlaps that of miRNAs, a characteristic that has been
148 widely documented for endogenous tRFs in both plants and mammalian cells[20,21]. To
149 further identify potential target genes of tRF-T11, we performed an *in silico*
150 prediction using two independent bioinformatic tools, IntaRNAv2[22] and
151 psRNATarget[23], followed by differential expression analysis based on the gene
152 expression profiles in normal and tumor ovarian tissue to prioritize the candidate
153 targets. As a result, the top three differentially expressed genes, namely transient
154 receptor potential cation channel subfamily A member 1 (*TRPA1*), tetraspanin 17
155 (*TSPAN17*) and secretogranin V (*SCG5*), with the minimum required energy to
156 hybridize with tRF-T11 at their 3' UTR regions of mRNA, were considered as the
157 potential targets for further experimental validation (Fig 2e). Among these three genes,
158 *TRPA1*, a new target recently unveiled by Takahashi *et al*[24] for cancer therapies,
159 which acts by triggering a noncanonical oxidative stress defense mechanism of tumor
160 suppression, was dramatically downregulated in A2780 cells (by approximately 75%)
161 in a dose-dependent manner by tRF-T11 mimic treatment (Fig 2j, g), while the

mRNA levels of the other two targets did not vary significantly (Fig 2f). Furthermore, a marked decrease of over 50% in the protein expression level of *TRPA1* was also observed in A2780 cells treated with tRF-T11 mimic (Fig 2h, i), which may act as a translational repressor of the *TRPA1* gene by acting like a miRNA in human OVCA cells. Indeed, previous reports revealed that *TRPA1* overexpression is associated with poor survival probability in patients (Fig 2k). Unfortunately, no clinical therapeutic drug targeting *TRPA1* is available, and our findings provide a novel RNA sequence derived from plant can potently silence human *TRPA1*.

Recently, advances in RNA therapeutics have been facilitated by breakthroughs in pharmaceutical delivery systems, including liposomes, nanoparticles, dendrimers and carbon nanotubes have been shown to provide promising application *in vitro* and *in vivo*[25]. To evaluate the antitumor activity *in vivo*, a histidine-lysine polymer (HKP) nanoparticle system was applied to deliver tRF-T11 mimic to a well-established xenograft mouse model of human OVCA cells. The mass ratio of HKP and tRF-T11 mimic was optimized (Fig 3a, b) with an appropriate particle size (164.2 nm) and good dispersion (41.2 mV, Fig 3c). As shown in Fig 3d to g, compared to vehicle

control group, tRF-T11 mimic treatment of xenografts for 20 days significantly diminished the tumor growth rate by approximately 50% at a dose of only 177 nmol/kg, which is more than 16-fold lower than that of taxol (2928 nmol/kg) required to achieve comparable tumor-suppressive effects without significant adverse impacts on body weight. Compared to those from control mice, the protein expression levels of *TRPA1* in the tumors with intratumoral injection of high-dose tRF-T11 mimic exhibited significant reduction (Fig 3h, i), which is consistent with the western blot results *in vitro*. Although taxol is a commonly used first-line drug for cancer patients, chemoresistance is usually observed. Since tRF-T11 mimic exhibited comparable tumor suppression efficacy to taxol at a much lower dose, our study may indicate an alternative treatment option.

In summary, this study provides the first evidence that plant-derived tRNAs and tRFs from Chinese yew exhibit potent antitumor effects against human OVCA, which will greatly expand our knowledge on the active ingredients in natural sources, and provide additional clues for evaluating the active components of medicinal plants or herbal medicines. Although cross-kingdom regulation in human by miRNA uptake

194 from food and medicinal plants has been widely studied, this report emphasizes the
195 potential regulatory roles of plant-derived small RNAs from an abundance of
196 housekeeping noncoding RNA species, such as tRNAs and tRFs. This infinitely vast
197 pool filled with RNA sequences and chemical modifications provided by nature can
198 serve as a new sequence library for the development of novel RNAi-based
199 therapeutics. Furthermore, since chemical modified oligonucleotides could be simply
200 and efficiently synthesized in large amount using the phosphoramidite
201 methodology[26,27], this discovery demonstrated a pilot strategy for identifying
202 pharmacologically active tRFs from plants, such as those from the genus *Taxus*.

203 As a promising and rapidly advancing frontier, siRNA can be readily designed
204 based on a well-validated target mRNA. Often, the process of unraveling the
205 pathogenesis of many human diseases to find key molecular targets for drug treatment
206 is time-consuming and difficult without a functional approach with bottom-up
207 guidance. As a result, the effective design of RNAi therapeutic drug candidates will
208 be difficult or impossible due to the lack of reliable targets. As a benefit of the high
209 target specificity and selectivity of RNA drugs, pharmacologically active RNA

molecules identified from medicinal plants could, in turn, lead to the improvement of the efficiency and possibilities of discovering new drug target, and shed light on disease etiology.

**Acknowledgements**

We thank Novogene Bioinformatics Institute (Beijing, China) for technical support in next-generation sequencing; Y. L. (Sirnaomics, Inc., U.S.A.) for technical advice and the gift of HKP for RNA delivery *in vivo*. This work was financially funded by the CUHK Direct Grant 4053364, the Innovation and Technology Commission, Hong Kong Government to the State Key Laboratory, and grant from The Science and Technology Development Fund, Macau SAR (File no. 015/2017/AFJ).

**Contributions**

Z.-H.J. and T.-M.Y. conceived the study. K.-Y.C., T.-M.Y. and T.-F.C. designed the experiments. K.-Y.C., T.-M.Y., J.-Z.Z. and J. L. conducted the experiments. K.-Y.C., J.-Z.Z. and C. L. analyzed the data. K.-Y.C., T.-M.Y. and E.L.L. drafted the manuscript. All authors approved the manuscript.

## Methods

**Plant materials and RNA extraction of *Taxus chinensis*.** Plants of *Taxus chinensis (Pilger) Rehd. var. mairei* (Lemee et Levl.) Cheng et L. K. Fu used in this study were collected from Sanming City, Fujian Province, China. Plant materials were freshly cut, frozen and stored in liquid nitrogen until use.

Plant tissues were ground into a fine powder in liquid nitrogen and were then homogenized (IKA, Germany) in CTAB buffer. After incubation for 2 min at 65°C, the tissue lysate was cooled immediately on ice for 10 min, followed by centrifugation at 12,000 ×g for 15 min at 4°C. The supernatant was collected and extracted with an equal volume of phenol:chloroform:isopentanol (50:48:1). Phases were separated at 4°C by centrifugation at 12,000 ×g for 15 min. The supernatant was extracted again as described above with chloroform:isopentanol (24:1) and mixed with an equal volume of 6 M guanidinium thiocyanate solution (Tokyo Chemical Industry, Japan) and ethanol (Anaqua Chemicals Supply, U.S.A.) to a final concentration of 55%. The mixture was passed through a silicon-membrane column and washed with 80% ethanol. Finally, total RNA was eluted with RNase-free water,

and small RNA species were enriched by using a mirVana miRNA isolation kit (Invitrogen, U.S.A.) following the manufacturer's instructions.

**tEF preparation.** Small RNA was separated by 6% urea-polyacrylamide gel electrophoresis (PAGE). Gel fractions containing the tEF, as visualized by SYBR Gold nucleic acid gel staining (Thermo, U.S.A.), were excised and electroeluted in 3 kD molecular weight cut off dialysis tubing (Spectrum, U.S.A.) at 100 V for 1.5 h. The tEF was finally desalted and recovered on a silicon-membrane column.

**tEF library construction and sequencing.** Sequencing libraries were generated by using a TruSeq small RNA Library Preparation Kit (Illumina, U.S.A.), followed by a round of adaptor ligation, reverse transcription and PCR. PCR products were then purified, and libraries were quantified on an Agilent Bioanalyzer 2100 system (Agilent Technologies, U.S.A.). The library preparations were sequenced at the Novogene Bioinformatics Institute (Beijing, China) on an Illumina HiSeq platform using the 150-bp paired-end (PE150) strategy to generate over 15 million raw paired

258 reads. A total of 1,729,438 clean reads were obtained by removing low quality
259 regions and adaptor sequences. The tRNA genes were identified by using the
260 tRNAscan-SE 2.0 program (http://lowelab.ucsc.edu/tRNAscan-SE/) and annotated by
261 searching the Nucleotide Collection (nr/nt) database using the Basic Local Alignment
262 Search Tool (BLAST) program (https://blast.ncbi.nlm.nih.gov/Blast.cgi).
263
264 **Purification of individual tRNAs.** Synthetic single-stranded DNA oligonucleotides
265 (BGI, China; Supplementary Table 3) complementary to the target tRNA were mixed
266 with *Taxus* small RNA and denatured at 95°C for 5 min, followed by incubation at a
267 temperature 5°C lower than the melting temperature (Tm) for 1.5 h. Streptavidin
268 magnetic beads (Beaverbio, China) were then added to the mixture and incubated for
269 30 min at the annealing temperatures. Then, the biotinylated DNA/tRNA-coated
270 beads were separated with a magnet and washed at 40°C. Subsequently, the magnetic
271 beads were resuspended in RNase-free water, and the immobilized tRNA with probes
272 was released by incubation at 65°C for 5 min. The solutions were directly injected
273 using an ACQUITY UPLC OST $C_{18}$ column (2.1×100 mm i.d., 1.7 μm; Waters,

U.S.A.) maintained at 60°C into a UHPLC Agilent 1290 system (Agilent, U.S.A.) equipped with a diode array detector. The flow rate was set at 0.2 mL/min, and a gradient elution was performed with (A) 100 mM HFIP+15 mM TEAA and (B) 50% MeOH in A as follows: 0-1.5 min, 2% B; 1.5-8.3 min, 2%-28% B; and 8.3-16.5 min, 28%-34% B. MS data were acquired on an Agilent 6545 Q-TOF mass spectrometer with a gas temperature of 320°C, spray voltage of 3.5 kV, and sheath gas flow and temperature of 12 L/min and 350°C, respectively. For the MS experiment, samples were analyzed in negative polarity over an m/z range of 500 to 3200. Fractions from chromatographic peaks of individual tRNAs were collected and freeze dried.

**RNA transfection and cytotoxicity determination.** RNA samples dissolved in RNase-free water were stored at -20°C before use. Transfection of RNA samples was performed according to the manufacturer's instructions for Lipofectamine RNAiMAX Transfection Reagents (Thermo, U.S.A.). After treatment for 48 h, an MTT assay was performed, and absorbance values were calorimetrically determined at 570 nm using a SpectraMax 190 microplate reader (Molecular Devices, Sunnyvale, U.S.A). The

290 dose-dependent $IC_{50}$ values were calculated by GraphPad Prism 5.0 (GraphPad,
291 U.S.A.). A siRNA (Forward: 5'-GGAGCGAUUUAGCCAAGAATT-3', Sense:
292 5'-UUCUUGGC UAAAUCGCUCCTT-3') was used as positive control. Each
293 experiment was carried out three times. The results are expressed as the means ±
294 standard deviations.
295
296 **Acquisition of fluorescence images of transfected FAM-labeled tRF-T11 mimic**
297 **in A2780 cells.** Briefly, $1\times10^5$ A2780 cells were seeded in glass bottom cell culture
298 dishes (Nest Biotechnology, China). The medium was discarded after 20 h, and 50
299 nM FAM-labeled tRF-T11 mimic (GenePharma, China) was transfected into the cells.
300 After 6 h, the transfection medium was discarded, and the cells were rinsed 3 times
301 with RPMI 1640 medium. For nuclear staining, cells were incubated with 1 mL of
302 Hoechst 33258 (Sigma, U.S.A.) for 10 min at 37°C, followed by washing with RPMI
303 1640 medium. For mitochondrial staining, cells were incubated with 1 mL of
304 MitoBeacon Red (GeneCopoeia, U.S.A.) for 30 min at 37°C, followed by washing
305 with RPMI 1640 medium. Fluorescence images were acquired with an API

306 DeltaVision Live-cell Imaging System (Applied Precision Inc., GE Healthcare Co.,

307 U.S.A.) and were captured at x60 magnification, scale bar, 25 μm.

308

309 **tRF-T11 target prediction and prioritization.** Previously described small RNA or

310 tRF target prediction methods and restriction criteria were applied in this study to

311 identify functional target genes of tRF-T11[28]. Specifically, the 3' UTR sequences of

312 all mRNAs retrieved from GENCODE (v23) and the sequence of tRF-T11 derived

313 from *Taxus* were firstly loaded into IntaRNAv2 and psRNATarget to predict the

314 potential targets. The top 10 overlapping targets predicted were then prioritized and

315 filtered by crosschecking their expression in tumor and normal ovarian tissues.

316 Accordingly, we first obtained the gene expression profiles for 379 OVCA tissues and

317 88 normal ovarian tissues from UCSC Xena, which contains curated comprehensive

318 batch-effect-adjusted pancancer genomic data[29]. Subsequently, EBSeq[30] was

319 employed to filter the target genes differentially expressed between tumor and normal

320 ovarian tissues. The predicted targets satisfying two criteria, fold change

321 (tumor/normal) > 2 and FDR < 0.1.

**Quantitative real-time PCR**. Total RNA was extracted from A2780 cells treatment with the tRF-T11 mimic for 48 h using TRIzol (Invitrogen, U.S.A.) on a silicon-membrane column. RNA was then reverse transcribed using the GoScript Reverse Transcription System (Promega, U.S.A.). Quantitative real-time PCR was performed on a high-productivity real-time quantitative PCR ViiA™ 7 system (Life Technologies, U.S.A.) using GoTaq® qPCR Master Mix (Promega, U.S.A.) according to the manufacturers' instructions. The PCR primers were synthesized commercially (BGI, China, Supplementary Table 4). All data are presented as the mean fold change values duplicated and normalized to $\beta$-actin expression using the $2^{-\Delta\Delta CT}$ method. Each experiment was carried out three times. The results are expressed as the means ± standard deviations.

**Western blot analysis**. A2780 cell lysates were collected after treatment with tRF-T11 mimic for 48 h, and protein extraction was carried out using RIPA buffer (Cell Signaling Technology, U.S.A.) supplemented with protease and phosphatase

338 inhibitor cocktails (Roche, Switzerland). Protein concentrations were then determined
339 by a BCA protein assay (Thermo, U.S.A.). Denatured proteins were separated by 8%
340 SDS-PAGE and transferred to nitrocellulose membranes, followed by blocking with 5%
341 bovine serum albumin (Thermo, U.S.A.) for 2 h. Membranes containing proteins were
342 incubated with primary antibody against *TRPA1* (1:500 dilution, Novus, U.S.A.) or
343 *β*-actin (1:1000 dilution, Santa Cruz, U.S.A.) overnight, followed by washing in
344 TBST and incubation with a fluorescent secondary antibody (Li-cor, U.S.A.) for
345 detection. Band intensities were measured using ImageJ and were normalized to those
346 of *β*-actin. The sequences of TRPA1_siRNA01, TRPA1_siRNA02 and the scrambled
347 control (GenePharma) are shown in Supplementary Table 5. Each experiment was
348 carried out three times. The results are expressed as the means ± standard deviations.
349
350 **Preparation of HKP-tRF-T11 mimic nanoparticles**. HKP (a gift from Dr. Yang Lu,
351 Sirnaomics, Inc., U.S.A.) dissolved in RNase-free water (240 μg/mL) were first
352 balanced overnight at 4°C. Equal volumes of tRF-T11 mimic solutions at a
353 concentration of 80 μg/mL were then mixed and incubated at room temperature for 30

min. The particle sizes and zeta potential of the resulting nanoparticles were then evaluated by a Malvern Zetasizer Nano ZS90 (Malvern Instruments, U.K.).

***In vivo* models for tumor therapy**. A2780 cells ($4.0\times10^6$) were injected subcutaneously into the armpits of 8-week-old BALB/c nude mice (Shanghai SLAC Laboratory Animal Co., Ltd., China). When the tumors reached 50 $mm^3$, the tumor-bearing nude mice were treated with different doses (71 nmol/kg, 177 nmol/kg) of tRF-T11 mimic (GeneDesign, Inc. Osaka, Japan) encapsulated with HKP and different doses of taxol (2928 nmol/kg or 5855 nmol/kg) via intratumoral injection once every three days. A group treated with HKP alone was established as a control. The animals were sacrificed on day 20. Tumor diameters were measured at the points of maximum length and maximum width with digital calipers. Tumor volumes were calculated by the following formula: volume=$(\text{width})^2\times\text{length}/2$. The data were statistically analyzed using GraphPad Prism 5.0. Animal care and use protocols were performed in compliance with the guidelines of the Ethics Committee of the College of Pharmaceutical Sciences, Southwest University.

370

## References


1. Wani, M.C., Taylor, H.L., Wall, M.E., Coggon, P. & McPhail, A.T. Plant antitumor agents. VI. The isolation and structure of taxol, a novel antileukemic and antitumor agent from *Taxus brevifolia*. *J. Am. Chem. Soc.* 93, 2325-2327 (1971).
2. Yarnell E. Synergy in herbal medicines: part 1. *J. Restor. Med.* 4, 60–73 (2015).
3. Wu, L., Fan, J., & Belasco, J.G. MicroRNAs direct rapid deadenylation of mRNA. *Proc. Natl. Acad. Sci.* 103, 4034–4039 (2006).
4. Standart, N. & Jackson, R.J. MicroRNAs repress translation of $m^7$Gppp-capped target mRNAs in vitro by inhibiting initiation and promoting deadenylation. *Genes Dev*. 21, 1975–1982 (2007).
5. Zhang, L. *et al*. Exogenous plant MIR168a specifically targets mammalian LDLRAP1: evidence of cross-kingdom regulation by microRNA. *Cell Res.* 22, 273-274 (2012).

6. Chin, A.R. *et al.* Cross-kingdom inhibition of breast cancer growth by plant miR159. *Cell Res*. 26, 217-228 (2016).

7. Zhou, Z. *et al.* Honeysuckle-encoded atypical microRNA2911 directly targets influenza A viruses. *Cell Res.* 25, 39-49 (2015).

8. Du, J.C. *et al*. Plant-derived phosphocholine facilitates cellular uptake of anti-pulmonary fibrotic HJT-sRNA-m7. *Sci. China-Life Sci*. 60, 1-11 (2017).

9. Teng, Y. *et al*. Plant-derived exosomal microRNAs shape the gut microbiota. *Cell Host Microbe* 24, 1-16 (2018).

10. Shekhawat M., Jahagirdar D., Yadav S. & Sharma N.K. Induction of apoptosis in HeLa by corn small RNAs. *Nutr. Cancer* 71, 1-11 (2019).

11. Barciszewska M.Z., Perrigue P.M. & Barciszewski J. tRNA – the golden standard in molecular biology. *Mol. Biosyst.* 12, 12-17 (2016).

12. Anderson P. & Ivanov P. tRNA fragments in human health and disease. *FEBS Lett.* 588, 4297-4304 (2014).

13. Yeung, M.L. *et al.* Pyrosequencing of small non-coding RNAs in HIV-1 infected cells: evidence for the processing of a viral-cellular double-stranded RNA hybrid. *Nucleic Acids Res.* 37, 6575-6586 (2009).

14. Saikia, M. *et al.* Angiogenin-cleaved tRNA halves interact with cytochrome c, protecting cells from apoptosis during osmotic stress. *Mol. Cell. Biol.* 34, 2450-2463 (2014).

15. Goodarzi, H. *et al.* Endogenous tRNA-derived fragments suppress breast cancer progression via YBX1 displacement. *Cell* 161, 790-802 (2015).

16. Tsurui, H. *et al*. Batchwise purification of specific tRNAs by a solid-phase DNA probe. *Anal. Biochem*. 221, 166–172 (1994).

17. Martinez, G., Choudury, S.G. & Slotkin, R.K. tRNA-derived small RNAs target transposable element transcripts. *Nucleic Acids Res.* 45, 5142-5152 (2017).

18. Loss-Morais, G., Waterhouse, P.M. & Margis, R. Description of plant tRNA-derived RNA fragments (tRFs) associated with argonaute and identification of their putative targets. *Biol. Direct* 8, 1-6 (2013).

19. Keam, S.P. & Hutvagner, G. tRNA-derived fragments (tRFs): Emerging new roles for an ancient RNA in the regulation of gene expression. *Life* 5, 1638-1651 (2015).

20. Maute, R.L. *et al*. tRNA-derived microRNA modulates proliferation and the DNA damage response and is down-regulated in B cell lymphoma. *Proc. Natl. Acad. Sci.* 110, 1404-1409 (2013).

21. Deng, J.F. *et al.* Respiratory syncytial virus utilizes a tRNA fragment to suppress antiviral responses through a novel targeting mechanism. *Mol. Ther*. 23, 1622-1629 (2015).

22. Mann, M., Wright, P.R. & Backofen, R. IntaRNA 2.0: enhanced and customizable prediction of RNA-RNA interactions. *Nucleic Acids Res*. 45, W435-W439 (2017).

23. Dai, X., Zhuang, Z. & Zhao, P.X. psRNATarget: a plant small RNA target analysis server (2017 release). *Nucleic Acids Res*. 46: W49-W54 (2018).

24. Takahashi, N. *et al*. Cancer cells co-opt the neuronal redoxsensing channel TRPA1 to promote oxidative stress tolerance. *Cancer Cell* 33, 985–1003 (2018).

25. Kesharwani, P., Gajbhiye, V. & Jain, N.K. A review of nanocarriers for the delivery of small interfering RNA. *Biomaterials* 33, 7138-7150 (2012).

26. Michelson, A.M. & Todd, A.R. Synthesis of a dithymidine dinucleotide containing a 3' : 5'-internucleotidic linkage. *J. Chem. Soc.* 2632–2638 (1955).

27. Beaucage, S.L. & Iyer, R.P. Advances in the synthesis of oligonucleotides by the phosphoramidite approach. *Tetrahedron*. 48, 2223-2311 (1992).

28. Babski, J. *et al*. Small regulatory RNAs in Archaea. *RNA Biol*. 11, 484-493 (2014).

29. Goldman, M. *et al*. The UCSC Xena Platform for cancer genomics data visualization and interpretation. *bioRxiv* 326470 (2018).

30. Leng, N. *et al*. EBSeq: an empirical Bayes hierarchical model for inference in RNA-seq experiments. *Bioinformatics* 29, 1035-1043 (2013).

## Figure Legends

**Figure 1.** *Taxus*-derived tRNAs exhibit cytotoxicity *in vitro*. **a**, *Taxus* tEF with liposomal transfection exhibited strong cytotoxicity on A2780 cells. **b**, Representative MTT image of the *Taxus* tEF with or without liposomal transfection. **c**, Read length distribution of the tEF determined by NGS was primarily between 60 and 80 mer. **d**, NGS read content analysis showed that 14% of the tEF was tRNA. **e**, Urea-PAGE analysis of the tEF, rRNA fragment and purified tEF. **f**, The cytotoxicity of purified tEF increased after rRNA fragment deletion. **g**, Representative UHPLC method for purification of $tRNA^{His(GUG)}$. **h**, Deconvolution mass spectrometry and urea-PAGE analysis of purified $tRNA^{His(GUG)}$. **i**, Deconvolution mass results of $tRNA^{Glu(UUC)}$, $tRNA^{Trp(CCA)}$. $tRNA^{Leu(CAA)}$ and $tRNA^{Arg(ACG)}$. **j**, MTT assay of the top five abundant tRNAs from Chinese yew on A2780, HepG2 and MCF-7 cells. **k**, Representative MTT image of individual tRNAs on A2780 cells. **l**, Dose-dependent investigation of $tRNA^{Trp(CCA)}$ on A2780 cells. The data are shown as the means ± SDs of 3 independent experiments. $^{**}P<0.01$, $^{***}P<0.001$, $^{****}P<0.0001$.

**Figure 2**. *Taxus*-derived tRF-T11 mimic inhibits human OVCA cell proliferation by targeting *TRPA1 in vitro*. **a,** Design of tRF mimic from 5' and 3' end of tRNA. **b**, Heatmap of the inhibition rate of 36 synthesized tRF mimics against A2780 and A2780T cells. **c**, Investigation of the dose dependency of tRF-T11 mimic and taxol against A2780, A2780T and IOSE80 cells. **d**, Fluorescent images capture of FAM labeled tRF-T11 mimic in A2780 cells. **e**, Summary of hybridization energies and differential expression analysis of predicted target genes identified by the IntaRNA and psRNATarget tools. **f**, qPCR validation of the mRNA levels of predicted targets of tRF-T11 in A2780 cells. **g**, tRF-T11 mimic decreased the mRNA levels of *TRPA1* in a dose-dependent manner. **h**, Western blot assay for the evaluation of *TRPA1* expression in A2780 cells treated with tRF-T11 mimic, siRNA against *TRPA1* (TRPA1_siRNA01, TRPA1_siRNA02) and scrambled control at 25 nM. Band intensities were measured using ImageJ and were normalized to those of $\beta$-actin (**i**). **j**, Putative tRF-T11 binding sites in the *TRPA1* 3' UTR. **k**, Overall survival probability of patients in the TCGA OVCA cohort. The data are shown as the means ± SDs of 3 independent experiments. $^{**}P<0.01$, $^{***}P<0.001$, $^{****}P<0.0001$.

**Figure 3.** *Taxus*-derived tRF-T11 mimic decreases OVCA tumor growth via targeting *TRPA1 in vivo*. **a,** Structure of HKP. **b**, Optimization of the mass ratio of tRF-T11 mimic and HKP. **c**, The particle sizes and zeta potential of the HKP-tRF-T11 mimic. **d**, Growth rate of tumors treated with tRF-T11 mimic, taxol and HKP alone. **e**, Quantification of body weights in each group. **f**, Images of each tumor. **g**, No significant difference in tumor weight was observed during treatment in the high-dose tRF-T11 mimic group and the low-dose taxol group. **h**, Representative western blot image of *TRPA1* protein levels in tumors of different treatment. **i**, Band intensity ratio of *TRPA1*/*β*-actin in tumors treated with different doses of tRF-T11 mimic (n=6 per group). The data are shown as the means ± SDs of 3 independent experiments excluding those shown in **c** (± SEM). *$P<0.05$, **$P<0.01$, ***$P<0.001$.

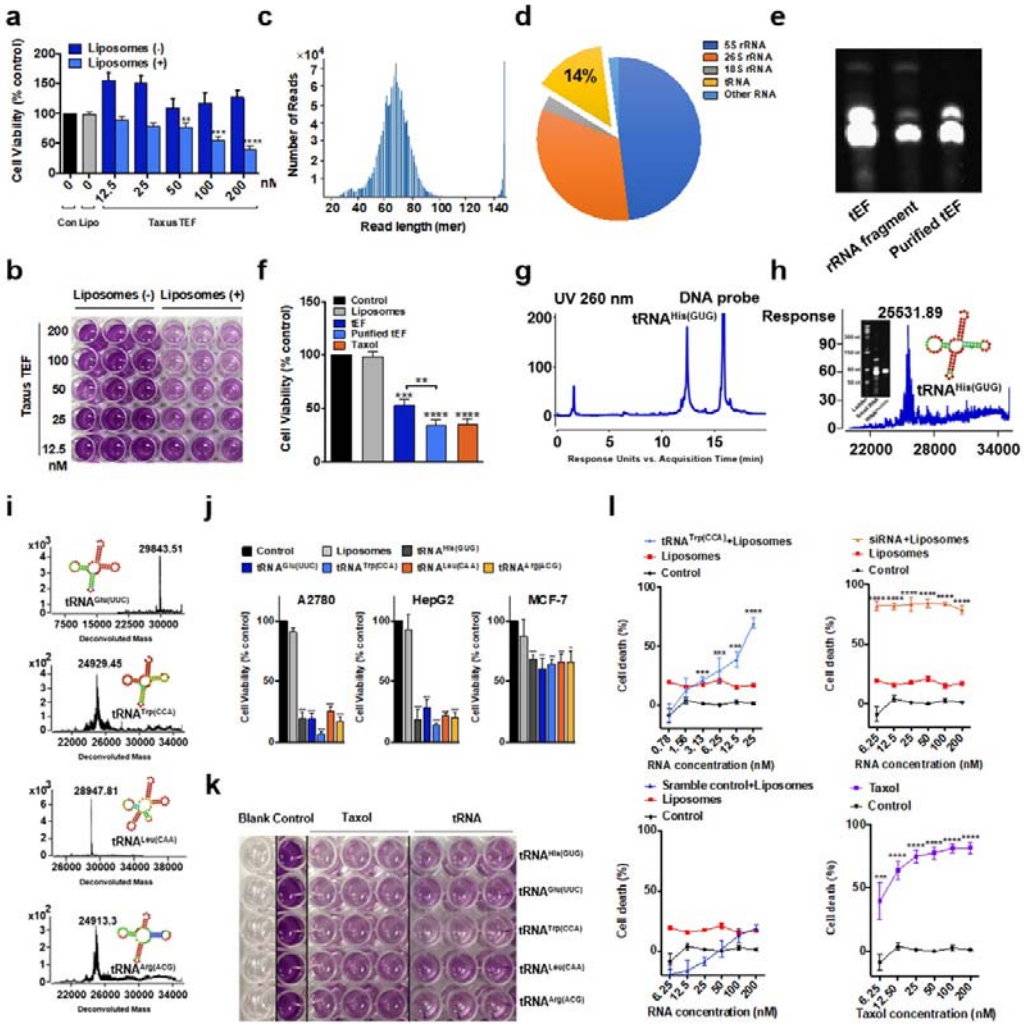
a
Liposomes (-)
Liposomes (+)
Cell Viability (% control)
Con Lipo
Taxus TEF
nM
c
Number of Reads
Read length (mer)
d
14%
5.5 rRNA
26.5 rRNA
18.5 rRNA
tRNA
Other RNA
e
tEF
rRNA fragment
Purified tEF
b
Liposomes (-) Liposomes (+)
Taxus TEF
nM
f
Control
Liposomes
tEF
Purified tEF
Taxol
Cell Viability (% control)
g
UV 260 nm
DNA probe
Response Units vs. Acquisition Time (min)
h
Response
25531.89
i
29843.51
24929.45
28947.81
24913.3
Deconvoluted Mass
j
A2780
HepG2
MCF-7
Cell Viability (% control)
k
Blank Control
Taxol
tRNA
l
Liposomes
Control
siRNA+Liposomes
Sramble control+Liposomes
Taxol
Cell death (%)
RNA concentration (nM)
Taxol concentration (nM)

**Figure 1**

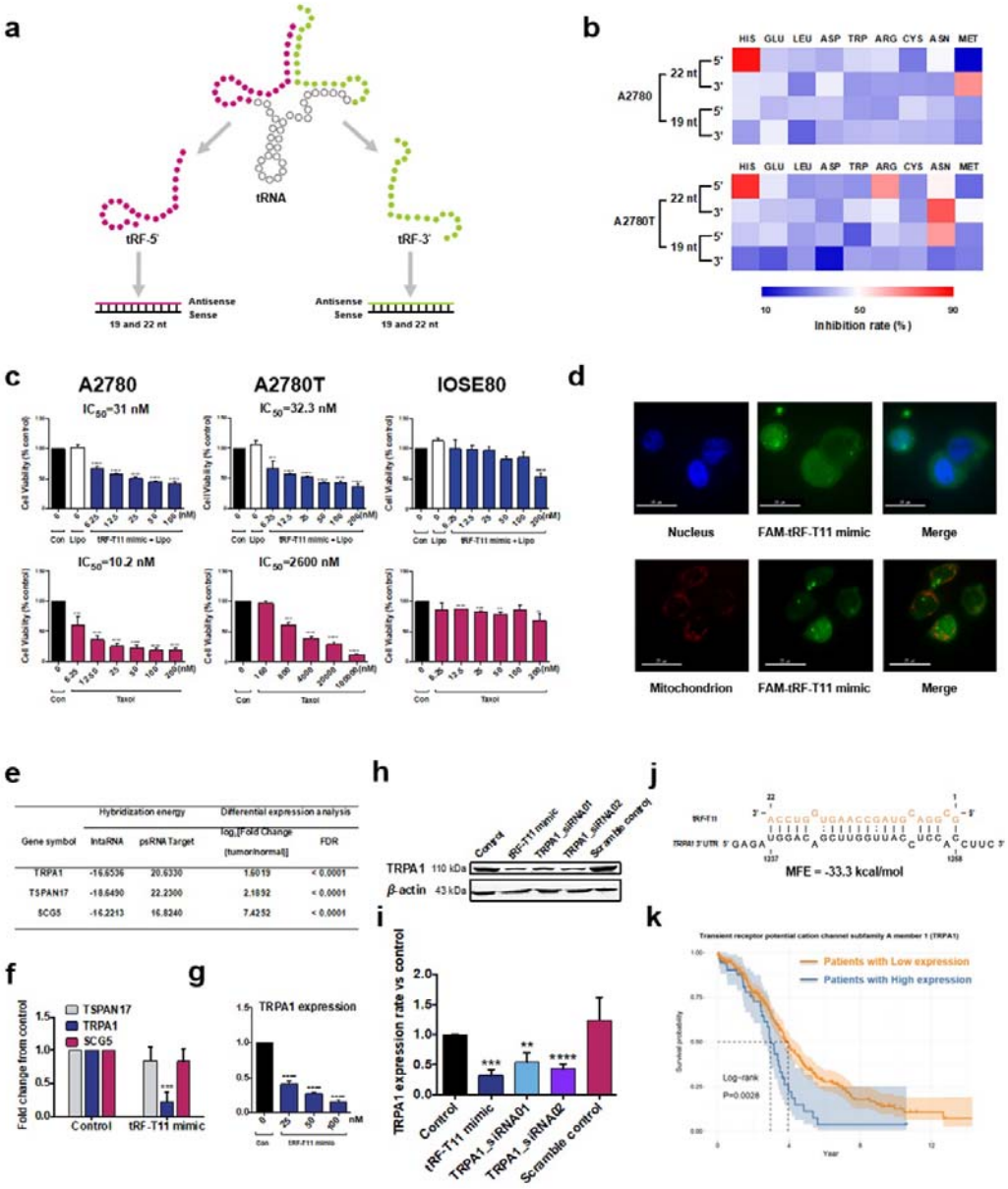
a
tRNA
tRF-5'
tRF-3'
Antisense
Sense
19 and 22 nt
b
HIS GLU LEU ASP TRP ARG CYS ASN MET
A2780
A2780T
22 nt
19 nt
Inhibition rate (%)
c
A2780
A2780T
IOSE80
IC50=31 nM
IC50=32.3 nM
IC50=10.2 nM
IC50=2600 nM
Cell Viability (% control)
Con
Lipo
tRF-T11 mimic + Lipo
Taxol
d
Nucleus
FAM-tRF-T11 mimic
Merge
Mitochondrion
e
Gene symbol
Hybridization energy
Differential expression analysis
IntaRNA
psRNA Target
log2(Fold Change (tumor/normal))
FDR
TRPA1
TSPAN17
SCG5
f
TSPAN17
TRPA1
SCG5
Fold change from control
Control
tRF-T11 mimic
g
TRPA1 expression
h
Control
tRF-T11 mimic
TRPA1_siRNA01
TRPA1_siRNA02
Scramble control
TRPA1 110 kDa
β-actin 43 kDa
i
TRPA1 expression rate vs control
j
MFE = -33.3 kcal/mol
k
Patients with Low expression
Patients with High expression
Log-rank
P=0.0028
Year

**Figure 2**

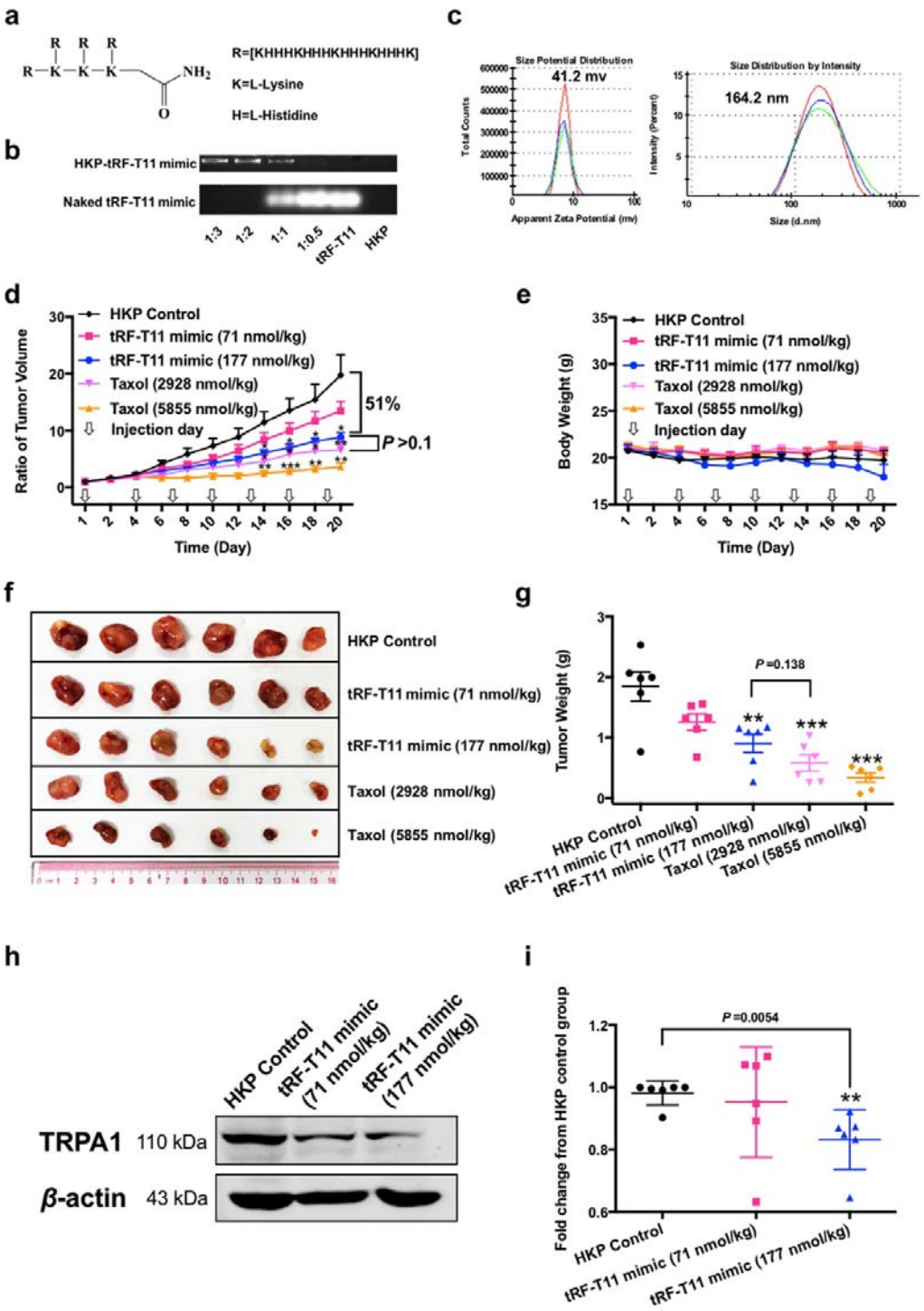
a
R=[KHHHKHHHKHHHKHHHK]
K=L-Lysine
H=L-Histidine
b
HKP-tRF-T11 mimic
Naked tRF-T11 mimic
1:3
1:2
1:1
1:0.5
tRF-T11
HKP
c
Size Potential Distribution
41.2 mv
Total Counts
Apparent Zeta Potential (mv)
Size Distribution by Intensity
164.2 nm
Intensity (Percent)
Size (d.nm)
d
HKP Control
tRF-T11 mimic (71 nmol/kg)
tRF-T11 mimic (177 nmol/kg)
Taxol (2928 nmol/kg)
Taxol (5855 nmol/kg)
Injection day
51%
P >0.1
Ratio of Tumor Volume
Time (Day)
e
Body Weight (g)
Time (Day)
f
HKP Control
tRF-T11 mimic (71 nmol/kg)
tRF-T11 mimic (177 nmol/kg)
Taxol (2928 nmol/kg)
Taxol (5855 nmol/kg)
g
P =0.138
Tumor Weight (g)
HKP Control
tRF-T11 mimic (71 nmol/kg)
tRF-T11 mimic (177 nmol/kg)
Taxol (2928 nmol/kg)
Taxol (5855 nmol/kg)
h
HKP Control
tRF-T11 mimic (71 nmol/kg)
tRF-T11 mimic (177 nmol/kg)
TRPA1 110 kDa
β-actin 43 kDa
i
P =0.0054
Fold change from HKP control group
HKP Control
tRF-T11 mimic (71 nmol/kg)
tRF-T11 mimic (177 nmol/kg)

**Figure 3**

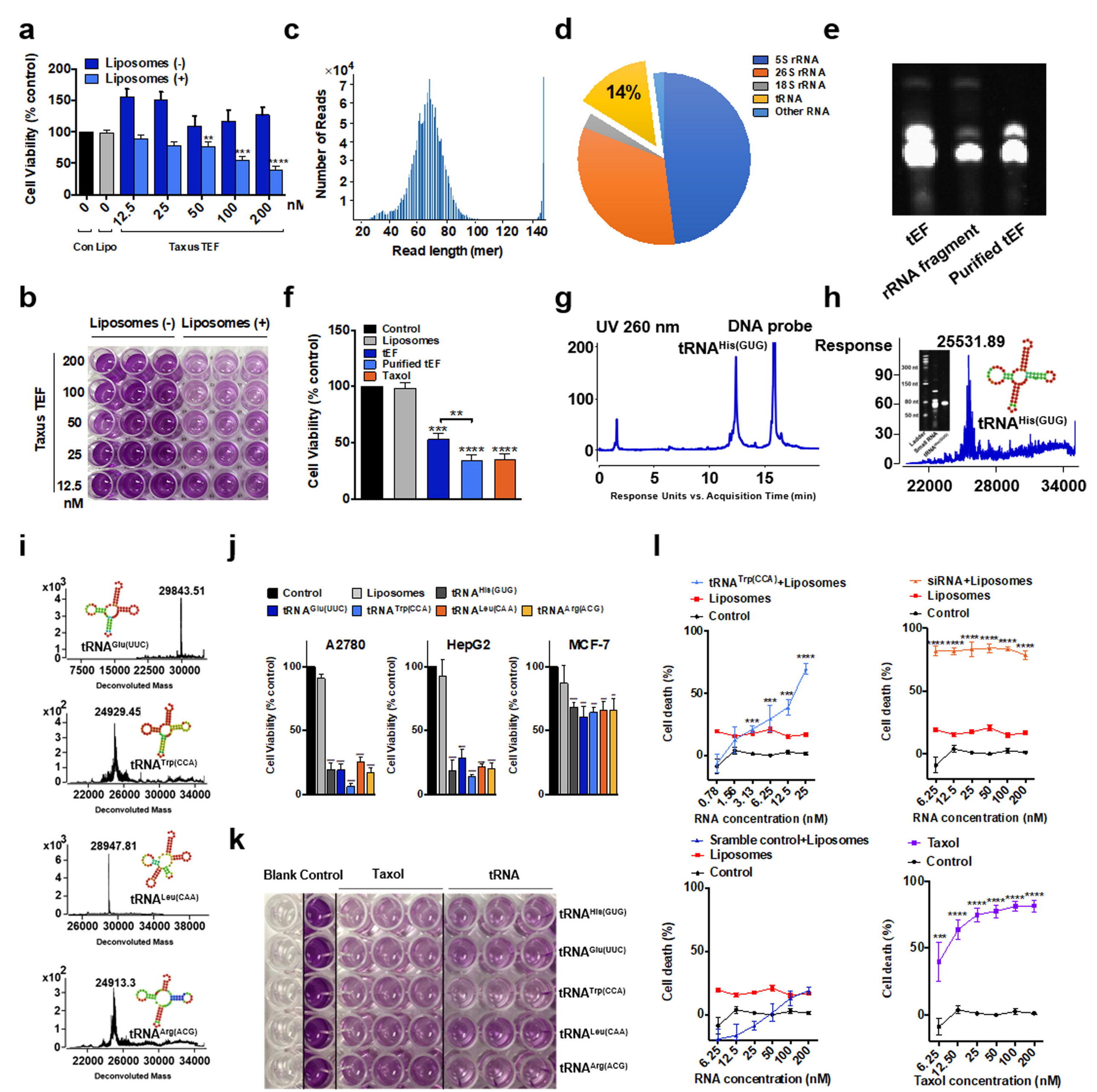
a
Liposomes (-)
Liposomes (+)
Cell Viability (% control)
Con Lipo
Taxus TEF
nM
b
Liposomes (-)
Liposomes (+)
Taxus TEF
nM
c
Number of Reads
Read length (mer)
d
14%
5S rRNA
26S rRNA
18S rRNA
tRNA
Other RNA
e
tEF
rRNA fragment
Purified tEF
f
Control
Liposomes
tEF
Purified tEF
Taxol
Cell Viability (% control)
g
UV 260 nm
DNA probe
tRNA His(GUG)
Response Units vs. Acquisition Time (min)
h
Response
25531.89
tRNA His(GUG)
i
29843.51
tRNA Glu(UUC)
Deconvoluted Mass
24929.45
tRNA Trp(CCA)
28947.81
tRNA Leu(CAA)
24913.3
tRNA Arg(ACG)
j
Control
Liposomes
tRNA His(GUG)
tRNA Glu(UUC)
tRNA Trp(CCA)
tRNA Leu(CAA)
tRNA Arg(ACG)
A2780
HepG2
MCF-7
Cell Viability (% control)
k
Blank Control
Taxol
tRNA
tRNA His(GUG)
tRNA Glu(UUC)
tRNA Trp(CCA)
tRNA Leu(CAA)
tRNA Arg(ACG)
l
tRNA Trp(CCA)+Liposomes
Liposomes
Control
siRNA+Liposomes
Sramble control+Liposomes
Taxol
Cell death (%)
RNA concentration (nM)
Taxol concentration (nM)

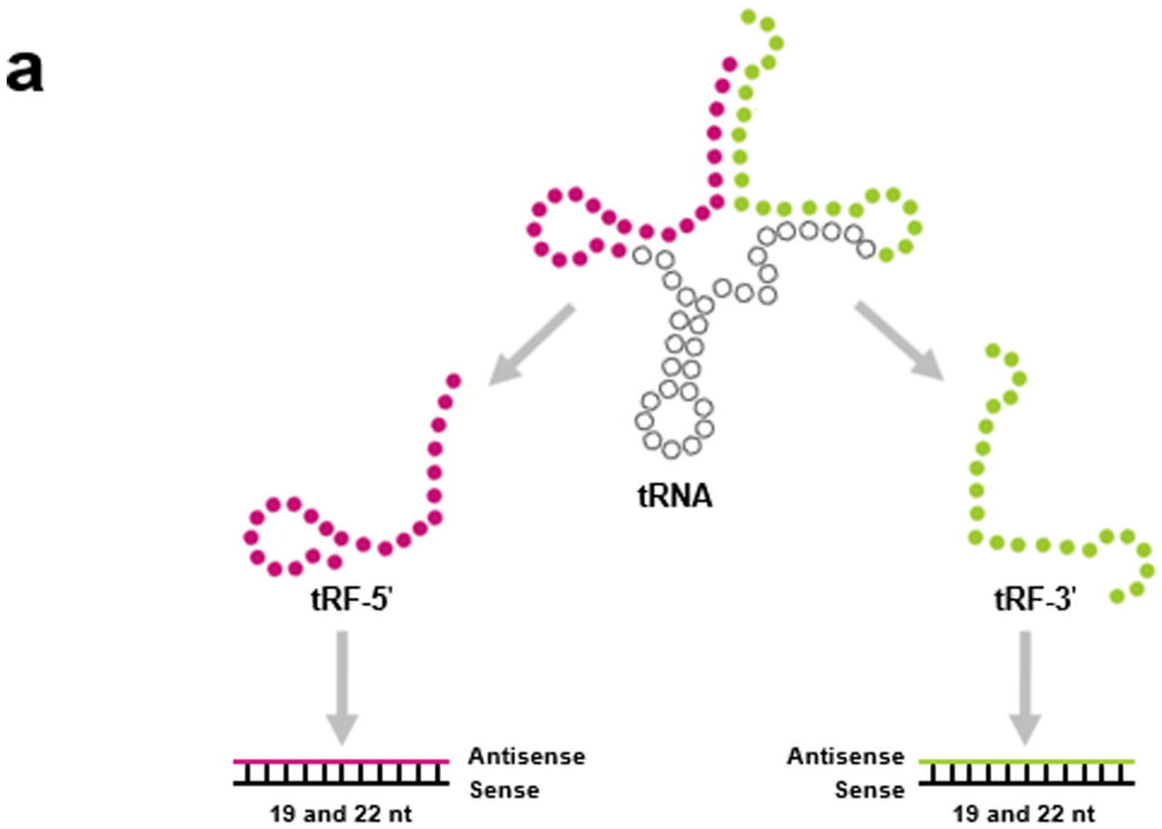


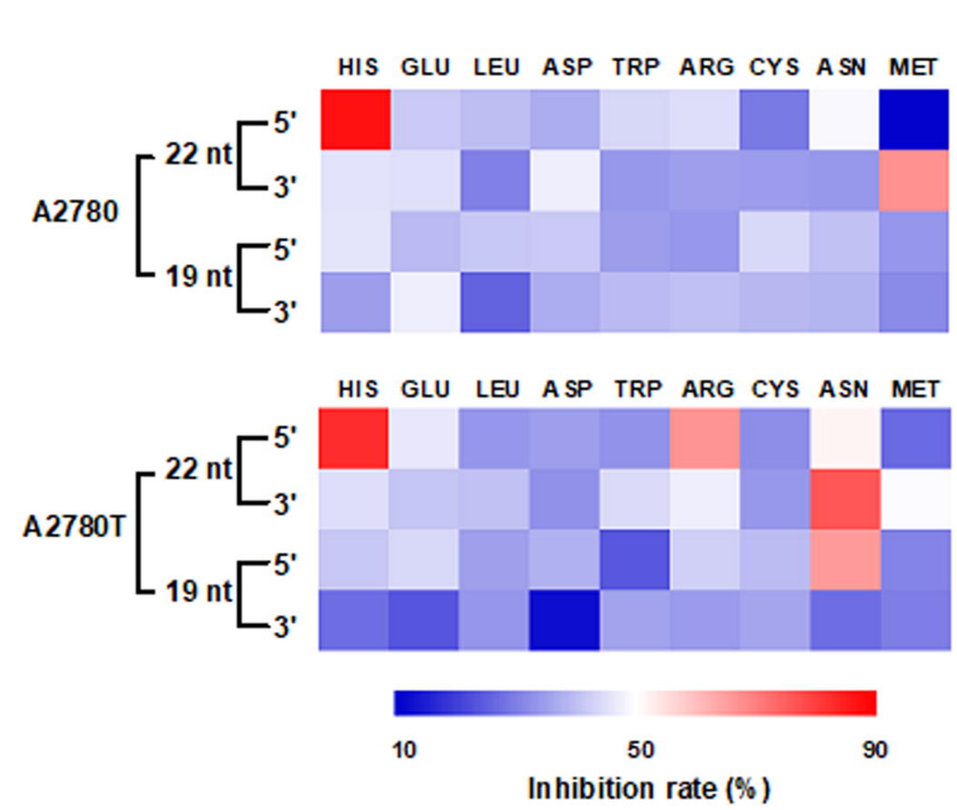


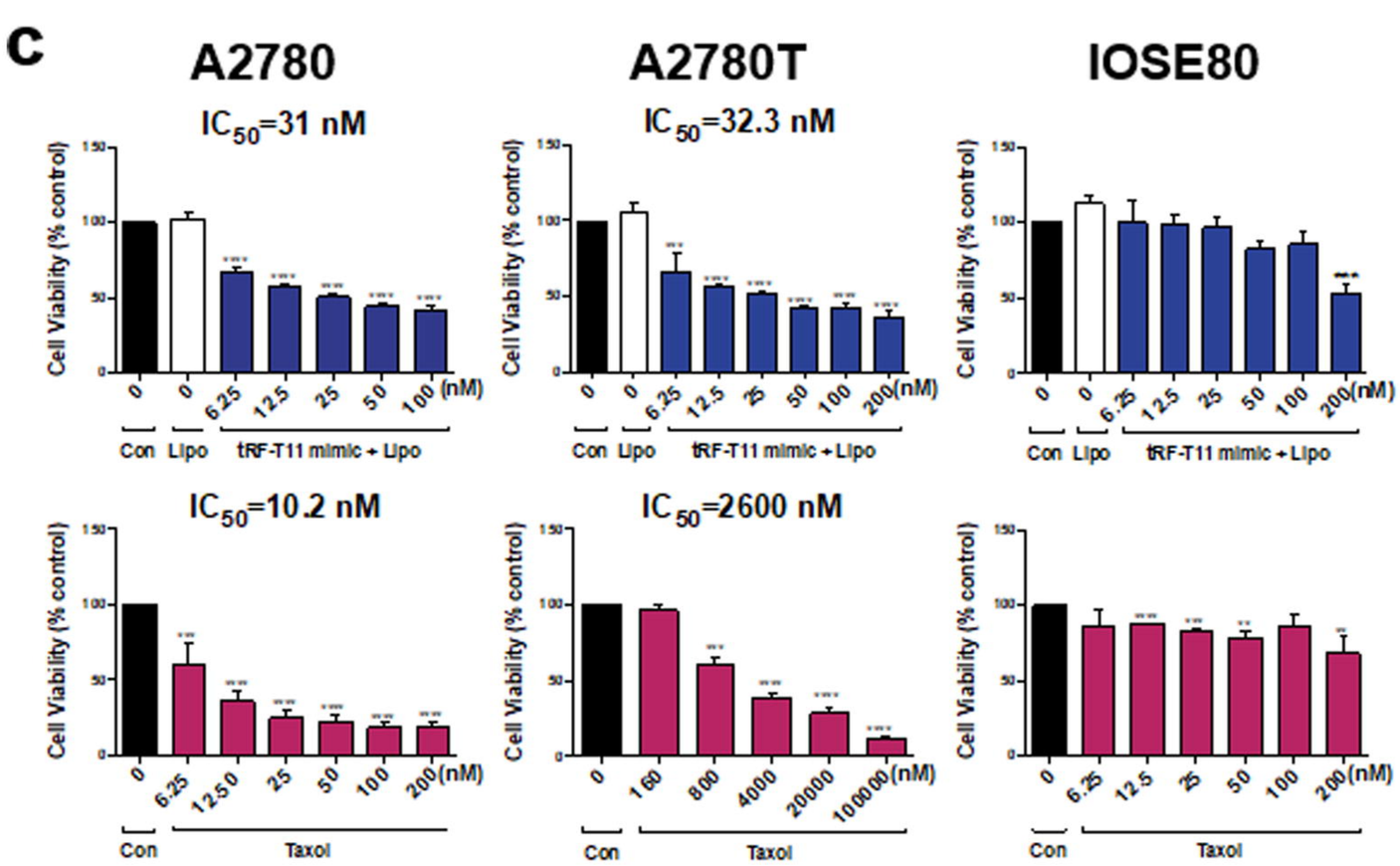


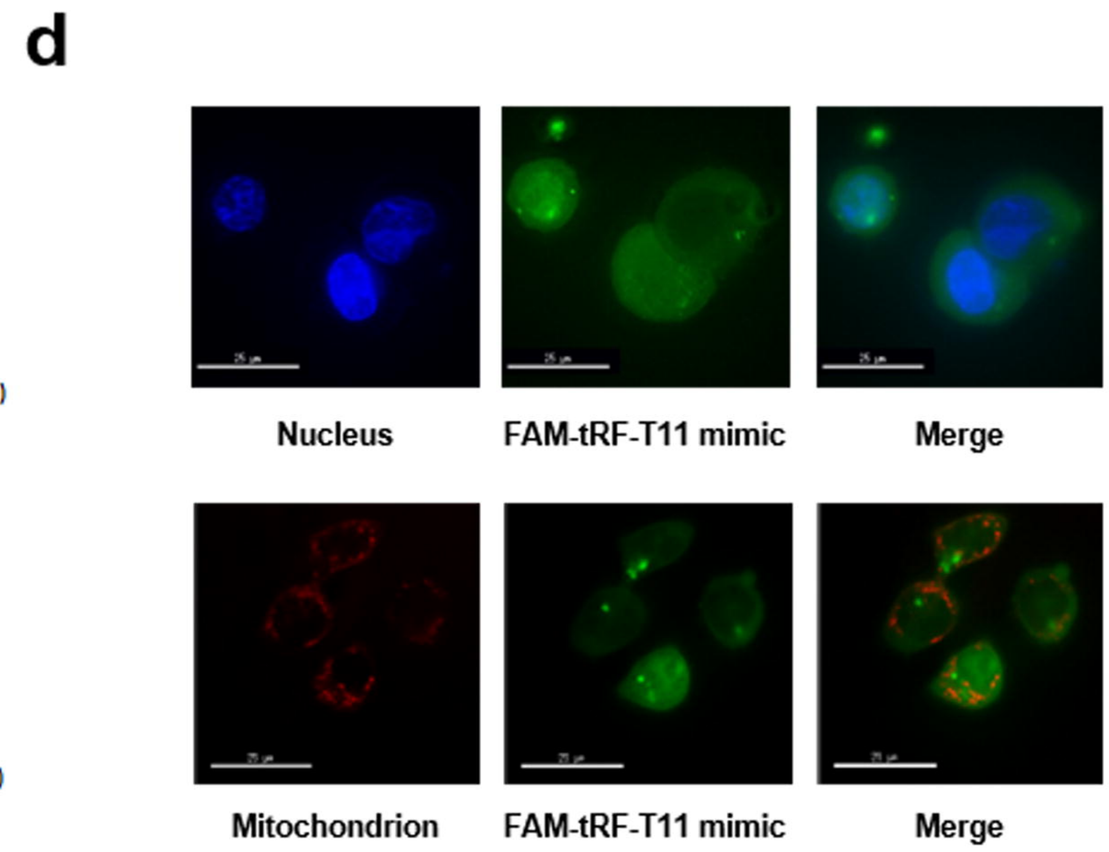


e

| Gene symbol | Hybridization energy | | Differential expression analysis | |
|---|---|---|---|---|
| | IntaRNA | psRNA Target | $log_2$[Fold Change (tumor/normal)] | FDR |
| TRPA1 | -16.6536 | 20.6330 | 1.6019 | < 0.0001 |
| TSPAN17 | -18.6490 | 22.2300 | 2.1892 | < 0.0001 |
| SCG5 | -16.2213 | 16.8240 | 7.4252 | < 0.0001 |

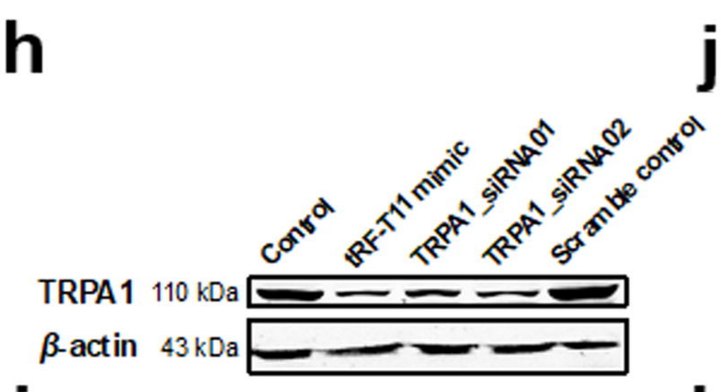


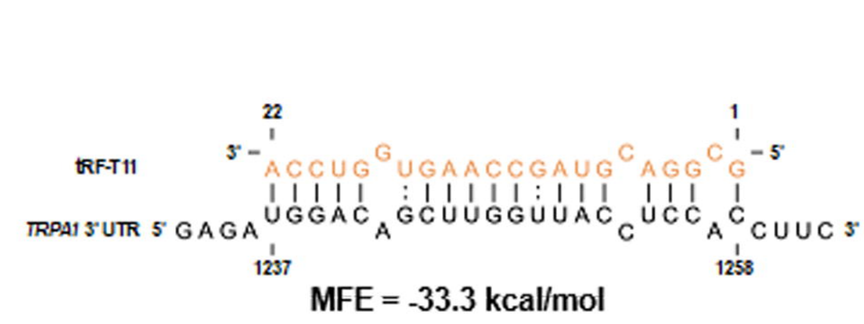


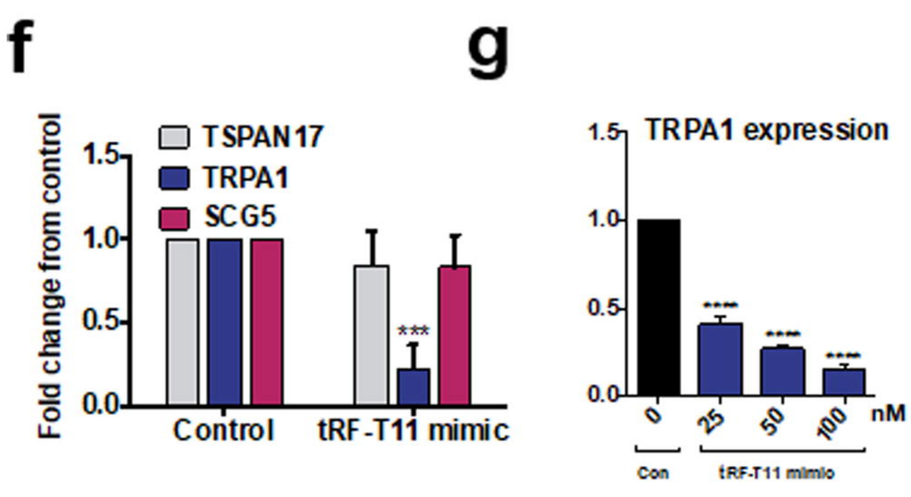


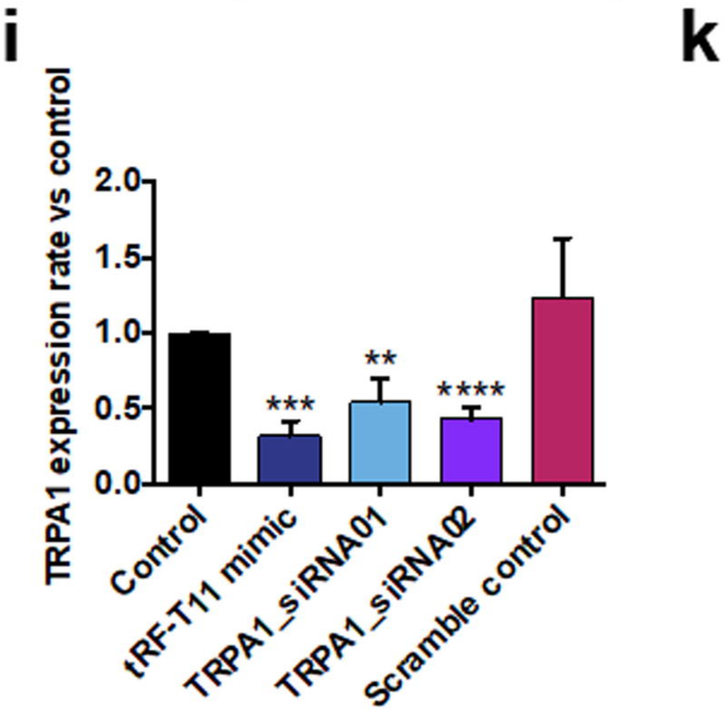


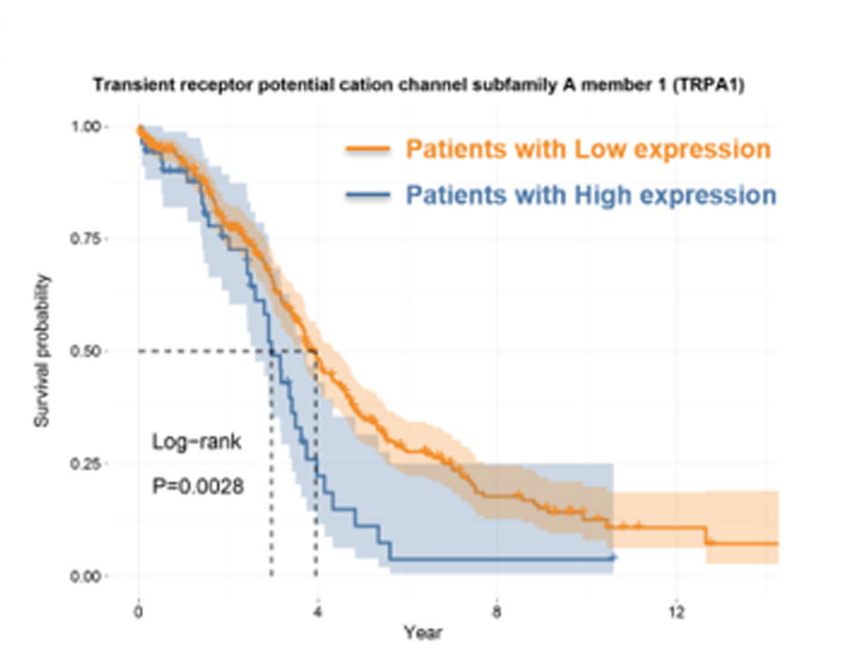

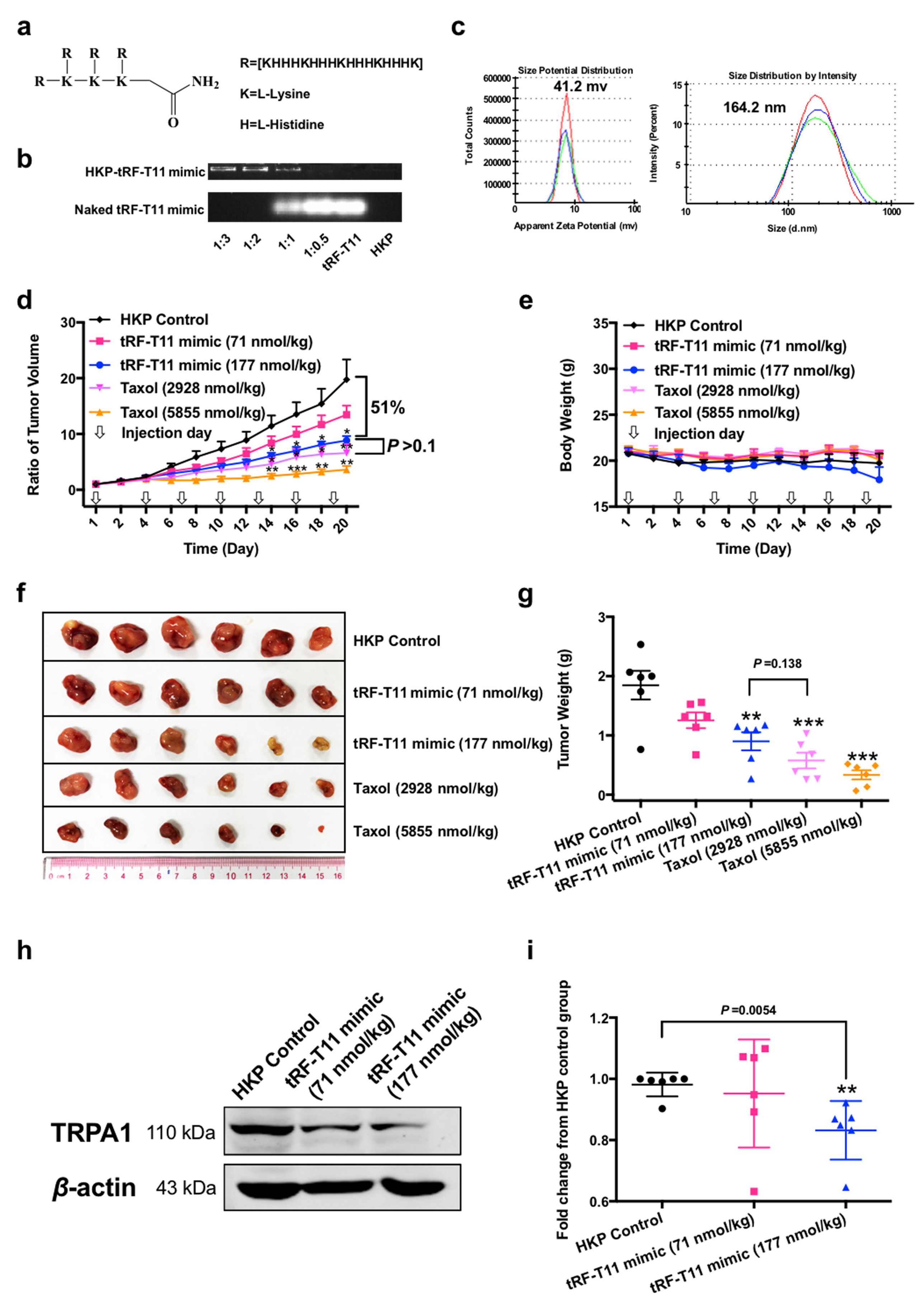
a
R=[KHHHKHHHKHHHKHHHK]
K=L-Lysine
H=L-Histidine
b
HKP-tRF-T11 mimic
Naked tRF-T11 mimic
1:3
1:2
1:1
1:0.5
tRF-T11
HKP
c
Size Potential Distribution
41.2 mv
Total Counts
Apparent Zeta Potential (mv)
Size Distribution by Intensity
164.2 nm
Intensity (Percent)
Size (d.nm)
d
HKP Control
tRF-T11 mimic (71 nmol/kg)
tRF-T11 mimic (177 nmol/kg)
Taxol (2928 nmol/kg)
Taxol (5855 nmol/kg)
Injection day
51%
P >0.1
Ratio of Tumor Volume
Time (Day)
e
Body Weight (g)
Time (Day)
f
HKP Control
tRF-T11 mimic (71 nmol/kg)
tRF-T11 mimic (177 nmol/kg)
Taxol (2928 nmol/kg)
Taxol (5855 nmol/kg)
g
P =0.138
Tumor Weight (g)
h
HKP Control
tRF-T11 mimic (71 nmol/kg)
tRF-T11 mimic (177 nmol/kg)
TRPA1 110 kDa
β-actin 43 kDa
i
P =0.0054
Fold change from HKP control group